AIAA JOURNAL
Vol. 43, No. 1, January 2005

Outflow Conditions for Integrated Large Eddy Simulation/Reynolds-Averaged Navier–Stokes Simulations

J. U. Schlüter,* H. Pitsch,† and P. Moin‡
Stanford University, Stanford, California 94305-3030

The numerical flow prediction of highly complex flow systems, such as the aerothermal flow through an entire aircraft gas turbine engine, requires the application of multiple specialized flow solvers, which have to run simultaneously in order to capture unsteady multicomponent effects. The different mathematical approaches of different flow solvers, especially large eddy simulation (LES) and Reynolds-averaged Navier–Stokes (RANS) flow solvers, pose challenges in the definition of boundary conditions at the interfaces. Here, a method based on a virtual body force is proposed to impose Reynolds-averaged velocity fields near the outlet of an LES flow domain in order to take downstream flow effects computed by a RANS flow solver into account. This method shows good results in the test case of a swirl flow, where the influence of a flow contraction downstream of the LES domain is represented entirely by the Reynolds-averaged velocity field at the outlet of the LES domain.

I. Motivation

NUMERICAL simulations of complex large-scale flow systems must capture a variety of physical phenomena in order to predict the flow accurately. Currently, many flow solvers are specialized to simulate one part of a flow system effectively, but are either inadequate or too expensive to be applied to a generic problem.

As an example, the aerothermal flow through a gas turbine engine can be considered. In the compressor and the turbine section, the flow solver has to be able to handle the moving blades, model the wall turbulence, and predict the pressure and density distributions properly. This can be done efficiently by a flow solver based on the Reynolds-averaged Navier–Stokes (RANS) approach. On the other hand, the flow in the combustion chamber is governed by large-scale turbulence, complex mixing processes, chemical reactions, and the presence of fuel spray. Experience shows that these phenomena require an unsteady approach.[1] Hence, the use of a large eddy simulation (LES) flow solver is desirable.

Although many design problems of a single-flow passage can be addressed by separate computations, only the simultaneous computation of all parts can guarantee the proper prediction of multicomponent phenomena, such as compressor/combustor instability and combustor/turbine hot-streak migration. Therefore, a promising strategy for performing full aerothermal simulations of gas turbine engines is the use of a RANS flow solver for the compressor sections, an LES flow solver for the combustor, and again a RANS flow solver for the turbine section (Fig. 1).

Previous work has established the communication and protocols for two different flow solvers running simultaneously to exchange flow data on the interfaces.[2–4] The processing of the obtained data to meaningful boundary conditions is discussed here for the LES outflow boundary.

II. Interface Boundary Conditions

The simultaneous computation of the flow in all parts of a gas turbine with different flow solvers requires an exchange of information at the interfaces of the computational domains of each part. The necessity of information exchange in the flow direction from the upstream to the downstream flow solver is self-explanatory: the flow in a passage is strongly dependent on mass flux, velocity vectors, and temperature at the inlet of the domain. However, because the Navier–Stokes equations are elliptic in subsonic flow, the downstream flow conditions can have a substantial influence on the upstream flow development. This can easily be imagined by considering that, for instance, a flow blockage in the turbine section of the gas turbine can determine and even stop the mass flow through the entire engine. This means that the information exchange at each interface has to go in both downstream and upstream directions.

Considering an LES flow solver computing the flow in the combustor, information on the flowfield has to be provided to the RANS flow solver computing the turbine as well as to the RANS flow solver computing the compressor; at the same time, the LES solver has to obtain flow information from both RANS flow solvers (Fig. 2). The coupling can be done using overlapping computational domains for the LES and RANS simulations. For the example of the combustor/turbine interface this would imply that inflow conditions for RANS will be determined from the LES solution at the beginning of the overlap region, and correspondingly the outflow conditions for LES are determined from the RANS solution inside the overlap region.

However, the different mathematical approaches of the different flow solvers make the coupling of the flow solvers challenging. Because LES resolves large-scale turbulence in space and time, the time steps between two iterations are relatively small. RANS flow solvers average all turbulent motions over time and predict ensemble averages of the flow. Even when a so-called unsteady RANS approach is used, the time step used by the RANS flow solver is still usually much larger than that for an LES flow solver.

The specification of boundary conditions for RANS from LES data is relatively straightforward. The LES data can be averaged over time and used as boundary condition for the RANS solver. The problem of specifying inflow conditions for LES from upstream RANS data is similar to that of specifying LES inflow conditions from experimental data, which are usually given in time-averaged form, and has therefore been investigated in some detail. A method that has been successfully applied in the past is, for instance, to generate a time-dependent database for inflow velocity profiles by performing a separate LES simulation, in which virtual body forces are applied to achieve the required time-averaged solution.[5] Current investigations aim to adapt this method to render the mean flow statistics flexible in order to take unsteady RANS solutions into account.[6,7]

In the present study the remaining flux of information from a downstream RANS computation to an upstream LES computation is investigated. LES computations have already shown that the flow

Presented as Paper 2002-3171 at the AIAA 32nd Fluid Dynamics Conference, St. Louis, MO, 24–27 June 2002; received 25 November 2002; accepted for publication 27 April 2004.

*Research Associate, Center for Turbulence Research. Member AIAA.
†Assistant Professor, Center for Turbulence Research. Member AIAA.
‡Professor, Center for Turbulence Research. Fellow AIAA.

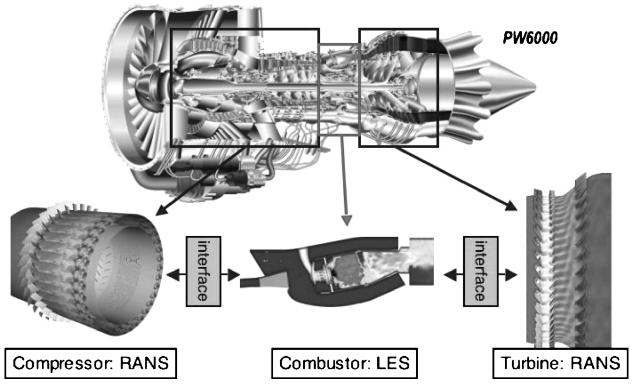

Fig. 1 Gas turbine engine.

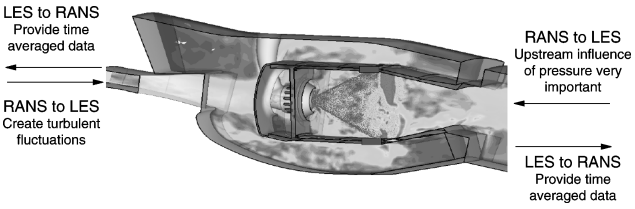

Fig. 2 Gas turbine combustor with interfaces.

can be sensitive to the outflow conditions.[8,9] The outflow conditions for LES have to be specified so that the time-averaged mean values of all computed quantities match the RANS solution at a given plane, but the instantaneous solution at the outflow still preserves the turbulent fluctuations.

III. Outflow Boundary Treatment

A natural choice to ensure a transfer of flow information from the downstream domain to the upstream domain would be to prescribe the outflow pressure distribution. However, modern LES flow solvers are often based on a low-Mach-number formulation. With this approximation, acoustic pressure fluctuations are neglected and the hydrodynamic pressure variations are determined by a Poisson equation. In this formulation, at the outflow, conditions are determined by the so-called convective outflow condition

$$\frac{\partial \phi}{\partial t} + u_c \frac{\partial \phi}{\partial n} = 0 \tag{1}$$

where ϕ is any scalar or velocity component, u_c is the convective velocity, and n is the coordinate in the direction of the outward normal at the boundary. The pressure at the outlet adjusts accordingly to the velocity distribution determined by the Poisson equation and, hence, it cannot be prescribed.

The method that will be investigated in the current study is to add virtual body forces to the right-hand side of the momentum equations inside the overlap region of the computational domains of the LES and the RANS flow solver. The goal is to drive the LES solution toward the mean velocity profiles of the RANS solution.

For a constant-density flow that is stationary in the mean, the body force is given by

$$F_i(\boldsymbol{x}) = \sigma(\langle \bar{u}_i \rangle_{\mathrm{RANS}}(\boldsymbol{x}) - \langle \bar{u} \rangle_{i,\mathrm{LES}}(\boldsymbol{x})) \tag{2}$$

where $\langle \bar{u}_i \rangle_{\mathrm{RANS}}$ is the vector of target velocities obtained from the RANS computation and $\langle \bar{u}_i \rangle_{\mathrm{LES}}$ is the vector of time-averaged velocities from the LES computation. The factor σ corresponds to an impedance associated with the strength of the body force.

The forcing term in Eq. (2) involves only mean velocities, while the corresponding momentum equation is solved for the instantaneous velocities. As a result, the mean velocities from the LES simulation are corrected without attenuating the resolved turbulent fluctuations. It will be shown later that, to achieve this goal, the averaging time for $\langle \bar{u} \rangle_{i,\mathrm{LES}}$ needs to be longer than the characteristic times of the turbulence. Equation (2) also shows that the forcing term tends to zero if the actual mean velocity from the LES approaches the target velocity, which is a consistency requirement. Note also that the RANS velocities are prescribed not only in one plane, but in the entire overlap region.

The choice of σ controls the characteristic response time of the LES solution to a change in the outlet boundary condition. If σ tends to zero, the body force becomes essentially ineffective, resulting in a drift of the outflow mean velocity profile toward the unforced solution. High values of σ lead to faster change to the desired velocity field, but may lead to numerical instabilities.

An estimate for an adequate choice of σ can be given by a one-dimensional analysis of the stationary Euler equations:

$$\frac{\partial u}{\partial t} + u \frac{\partial u}{\partial x} = -\frac{\partial p}{\partial x} + \sigma(\langle \bar{u} \rangle_{\mathrm{RANS}} - \langle \bar{u} \rangle_{\mathrm{LES}}) \tag{3}$$

To simplify the equation, we assume a zero pressure gradient and a constant convection velocity with the bulk velocity u_B. Furthermore, the flow is stationary, which makes $\langle \bar{u} \rangle_{\mathrm{LES}} = u$. With $\langle \bar{u} \rangle_{\mathrm{RANS}} = u_t$, the target velocity in Eq. (3) becomes

$$u_B \frac{\partial u}{\partial x} = \sigma(u_t - u) \tag{4}$$

This ordinary differential equation can be solved analytically and leads to the following expression for u:

$$u(x) = u_t + (u_0 - u_t) \exp[-(\sigma/u_B)x] \tag{5}$$

with u_0 being the velocity at the beginning of the forcing region.

We now want to determine σ so that at the end of the forcing region at $x = l_F$ the velocity difference is smaller than the relative error:

$$\epsilon = |u(l_F) - u_t|/u_t] \tag{6}$$

Thus, Eq. (5) leads to

$$\sigma_{\min} = (u_B/l_F)\, \ell_n(|u_0 - u_t|/\epsilon u_t) \tag{7}$$

Although this estimate for σ ensures the accuracy of the approach for steady flows, in truly unsteady coupled computations a higher value for σ should be used to decrease the time-lag in which the flow solution adjusts to the target velocity obtained from an unsteady downstream computation.

On the upper end, σ is limited by numerical stability. Here, it is useful to write σ as an inverse time-scale τ_F. The upper limit is then defined corresponding to the Courant–Friedrichs–Lewy condition:

$$\sigma_{\max} = (1/\tau_F)_{\max} = u_c/\Delta x_F \tag{8}$$

with Δx_{F} being the size of the smallest cell in the forcing region and u_c the local convection velocity in this cell.

IV. Large Eddy Simulation Flow Solver

To test the body force for a boundary treatment, this method was implemented into an LES flow solver. The LES flow solver developed at the Center for Turbulence Research by Pierce and Moin[9] has been used. The flow solver solves the filtered momentum equations with a low-Mach-number assumption on an axisymmetric structured mesh. A second-order finite-volume scheme on a staggered grid is used.[10]

The subgrid stresses are approximated with an eddy-viscosity approach. The eddy viscosity is determined by a dynamic procedure.[11,12] For numerical purposes a convective boundary condition is applied at the outlet plane of the LES domain.

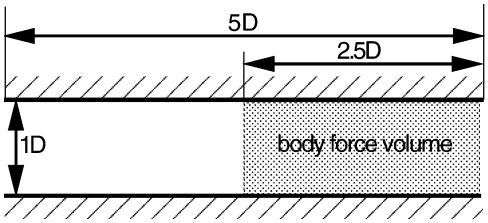

Fig. 3 Geometry of the pipe test case.

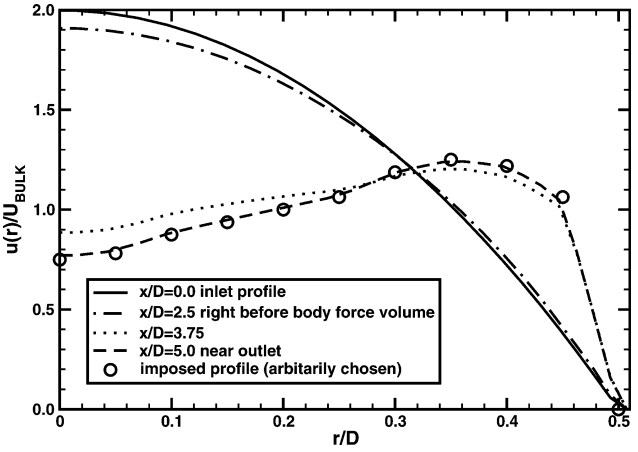

Fig. 4 Laminar pipe flow: radial profiles of axial velocity component $\langle \bar{u} \rangle_x$.

V. Numerical Experiment: Pipe Flow

To prove the feasibility and the well-posedness of this approach, a pipe flow has been computed (Fig. 3). The pipe has a length of five times the diameter D and the virtual body force is applied in a volume of length $2.5D$ at the end of the pipe flow to force the flow to a solution that would not naturally occur in this flow. The mesh consists of $128 \times 32 \times 64$ cells.

A. Laminar Flow: Feasibility

As a first step, a laminar pipe flow at a Reynolds number $Re = 10^3$ is considered. Figure 4 shows the resulting velocity profiles. The solid line shows the parabolic inlet profile corresponding to the solution of a fully developed pipe flow. Without forcing, this would be the solution at any downstream location in the pipe. The circles denote an arbitrarily chosen velocity profile, with the same mass flow rate as the inlet profile, which is to be matched at the outlet, considering these two velocity profiles as the initial and the target velocity. For a desired accuracy of 1% ($\epsilon = 0.01$) this leads to

$$\sigma_{\min} = \frac{1.0}{2.5} \cdot \ell_n \left(\frac{|2.0 - 0.75|}{0.01 \cdot 0.75} \right) = 2.05 \tag{9}$$

$$\sigma_{\max} = \frac{1.0}{5.0/128} = 25.6 \tag{10}$$

For all pipe flows computed here, σ was chosen to be $\sigma = 6.0$, except as stated otherwise.

Figure 4 shows the effect of the body force on the flow development. The dash-dotted line is a profile just upstream of the forcing region. The profile is different from the inflow solution, indicating that forcing influences the flowfield even upstream of the forcing region. After applying the virtual body force, the computed velocity profile quickly converges towards the imposed velocity profile.

B. Robustness Against Choice of σ

To show the robustness of the method for the choice of σ, several computations were performed with varying σ. Figure 5 shows

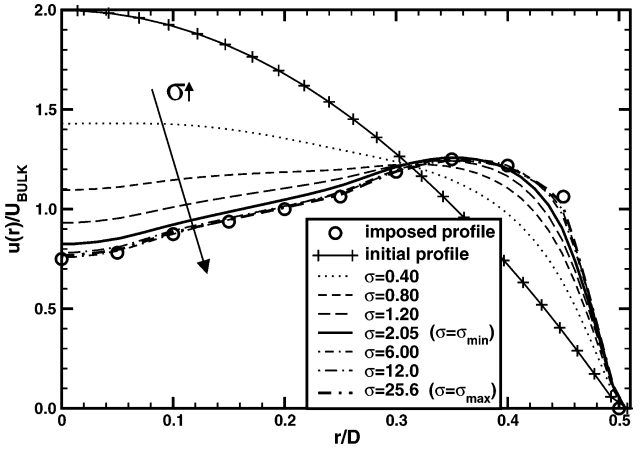

Fig. 5 Laminar pipe flow: profiles of axial velocity at the outlet ($x/D = 5.0$) in dependence on body force constant σ.

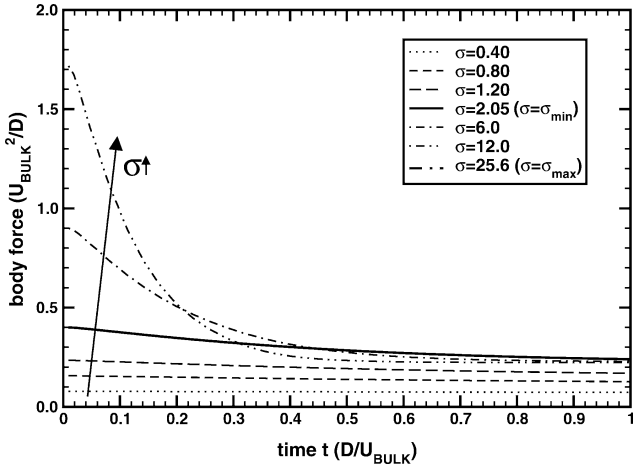

Fig. 6 Laminar pipe flow: temporal development of body force in the outlet plane in dependance of body force constant σ.

that with increasing σ the accordance of the LES solution with the imposed profile improves. The solutions using $\sigma \geq \sigma_{\min}$ show satisfactory results. Computations using $\sigma = 35.0 > \sigma_{\max}$ resulted in a diverging solution.

The temporal development of the body force dependent on the body force constant σ is shown in Fig. 6. Here, the spatial average of the body force in the outlet plane is computed and normalized with the bulk velocity and the diameter. Above the minimum σ the body force converges to the same residual body force that is needed to uphold the enforced velocity distribution. A higher body force allows the solution to converge in a shorter period of time.

C. Robustness Against Mass Conservation

An important test for consistency and well-posedness is the enforcement of a velocity profile that does not conserve mass. The exchange of the velocity profiles between RANS and LES flow solvers may introduce numerical errors, especially due to the interpolation between two different meshes, which could accumulate over time. In order to investigate the behavior of the proposed LES outflow conditions when this problem is encountered, an additional computation was made, where a "nonconservative" velocity profile, with a different mass flow rate, was used in the forcing. Figure 7 shows the resulting velocity profiles. The squares denote the imposed velocity profile, which clearly underestimates the mass flux. However, the computed velocity profile at the end of the forcing region has the same mass flux as the inlet profile. This shows that the method is

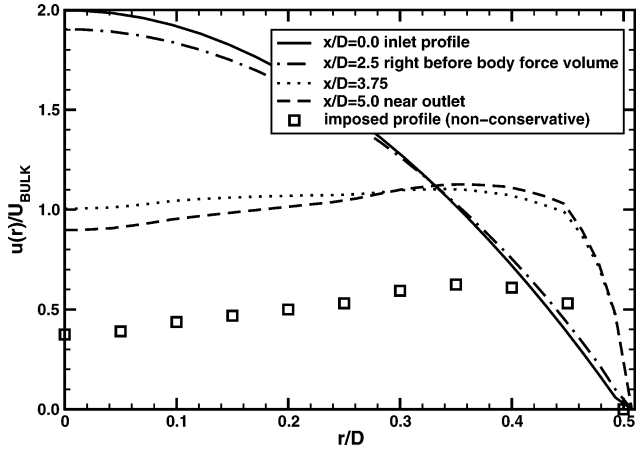

Fig. 7 Laminar pipe flow: profiles of axial velocity component. Nonconservative velocity profile imposed.

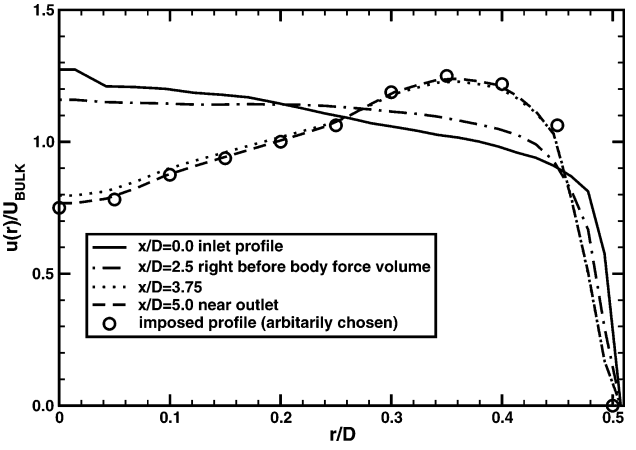

Fig. 8 Turbulent pipe flow: radial profiles of axial velocity component $\langle\bar{u}\rangle_x$. Averaging for $\langle\bar{u}\rangle_{\mathrm{LES}}$ using trailing time-window $\Delta t = 1.0$.

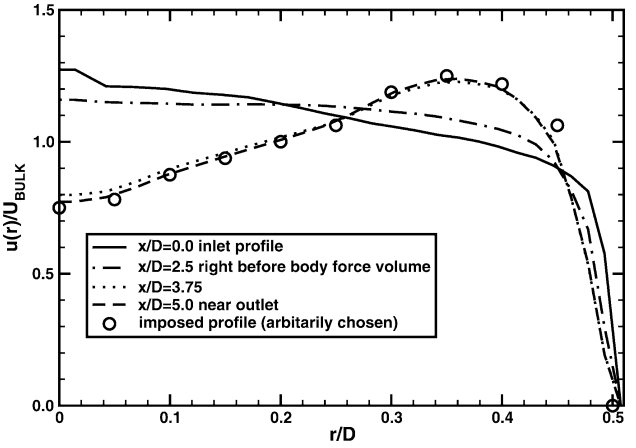

Fig. 9 Turbulent pipe flow: radial profiles of axial velocity component $\langle\bar{u}\rangle_x$. No averaging used [$\langle\bar{u}\rangle_{\mathrm{LES}} = u(t)$].

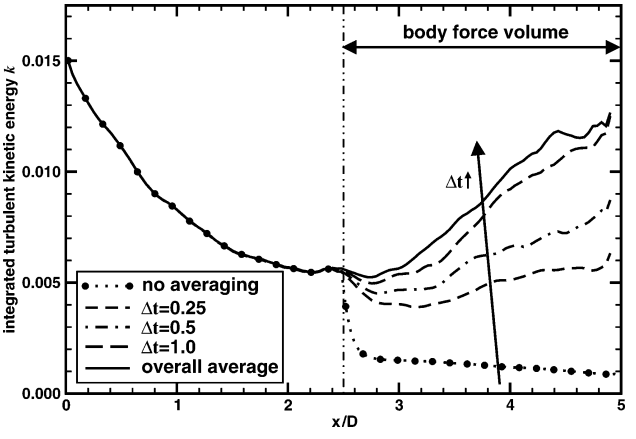

Fig. 10 Turbulent pipe flow: axial development of turbulent kinetic energy $k = \frac{1}{2}(\sqrt{u'^2} + \sqrt{v'^2} + \sqrt{w'^2})$ integrated over the cross section.

robust against inaccuracies resulting from the exchange of velocity profiles.

D. Turbulent Flow: Choice of Averaging Time-Span for $\langle\bar{u}_i\rangle_{\mathrm{LES}}$

The next test case considered here is a turbulent pipe flow at Reynolds number $Re = 15 \times 10^3$. The inflow conditions were created by an auxiliary LES computation of a periodic turbulent pipe flow recording a data base for the actual computation. The nondimensionalized bulk velocity at the inlet is $u_B = 1.0$ and the turbulence level is 10%.

Applying the proposed correction of the LES outflow by virtual body forces to this problem leads to the question of how to define the mean value $\langle\bar{u}\rangle_{\mathrm{LES}}$ of the LES computation. Several approaches have been tested:

1) Actual velocity $\langle\bar{u}\rangle_{\mathrm{LES}} = u(t)$: this results in a strong damping of turbulent fluctuations, because fluctuations of the velocity obviously lead to a counteracting virtual body force.

2) Overall mean value

$$\langle\bar{u}\rangle_{\mathrm{LES}} = \frac{1}{t - t_0}\int_{t_0}^{t} u(t)\,\mathrm{d}t$$

this ensures the least interference with turbulent fluctuations, but does not allow for unsteadiness in the mean profiles.

3) Averaging over a trailing time window

$$\langle\bar{u}\rangle_{\mathrm{LES}} = \frac{1}{\Delta t}\int_{t-\Delta t}^{t} u(t)\,\mathrm{d}t$$

here, it has to be ensured that Δt is long enough to average the turbulent fluctuations, but short enough to allow for unsteadiness of the mean profiles.

To determine the influence of the choice of the averaging timespan, several computations were performed with varying approaches and varying length of the trailing average. Figure 8 shows the mean velocity field for using a trailing time-window of length $\Delta t = 1.0$ for determining $\langle\bar{u}_i\rangle_{\mathrm{LES}}$. Because velocity difference on the axis is smaller than in the laminar case, the minimum forcing factor decreases to $\sigma_{\min} = 1.68$. Because the actual forcing parameter remained constant at $\sigma = 6.0$, the flow adjusts to the new velocity profile quicker.

Figure 9 shows the mean velocity profiles for a turbulent pipe flow using no averaging [$\langle\bar{u}\rangle_{\mathrm{LES}} = u(t)$]. As can be seen, the mean velocity field is indistinguishable from the previous computation.

However, there are some remarkable differences in the turbulent fluctuations. Figure 10 shows the axial development of the turbulent kinetic energy integrated over the cross section. At the inlet, the level of turbulent kinetic energy corresponds to the defined inflow conditions.[8] In the first half of the pipe, the level then decreases to a level corresponding to the natural state for the chosen parameters.

In the second half of the pipe, the body force is employed. Because of the new shape of the velocity profile, which possesses two additional inflection points and higher radial velocity gradients, the turbulence level increases, if approach 2, the overall mean, is used. Using approach 1 results in nearly complete attenuation of the turbulence. Employing a trailing time-window for the determination of $\langle\bar{u}_i\rangle_{\mathrm{LES}}$ improves the turbulence levels if the trailing window is sufficiently long.

The same trend can be seen in the radial distribution of the turbulent kinetic energy (Fig. 11) and the shear stresses (Fig. 12).

Here, averaging over one nondimensional time unit, given by the ratio of pipe diameter and bulk velocity, was found to be sufficient. This seems reasonable, because the previously mentioned criteria require the averaging time to be on the order of the Eulerian integral

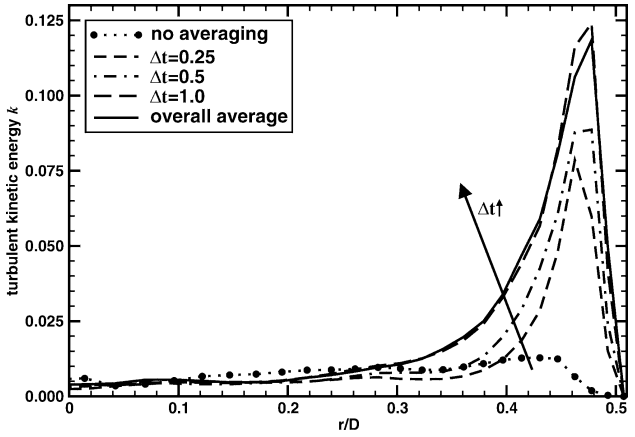

Fig. 11 Turbulent pipe flow: radial profiles of turbulent kinetic energy $k = \frac{1}{2}(\sqrt{u'^2} + \sqrt{v'^2} + \sqrt{w'^2})$ at the outlet ($x/D = 5.0$) for different averaging time span for $\langle \bar{u}_i \rangle_{\mathrm{LES}}$.

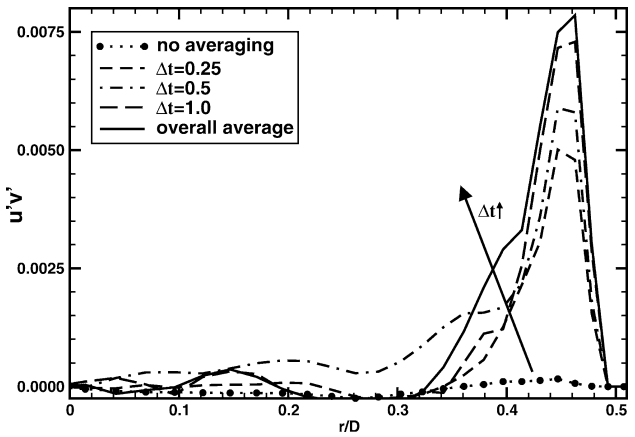

Fig. 12 Turbulent pipe flow: radial profiles of shear stress $\overline{u'v'}$ at the outlet ($x/D = 5.0$) for different averaging time-span for $\langle \bar{u}_i \rangle_{\mathrm{LES}}$.

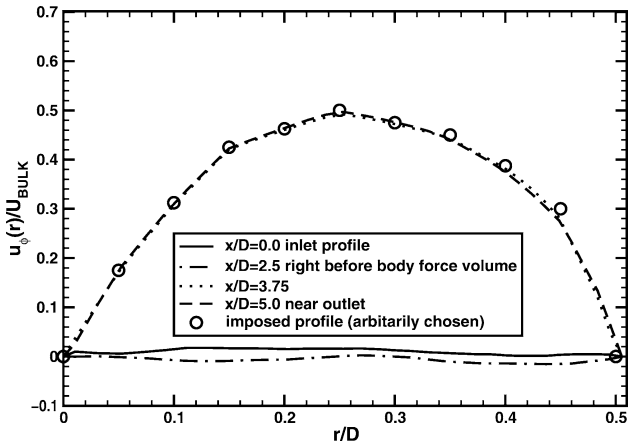

Fig. 13 Turbulent pipe flow: radial profiles of azimuthal velocity component $\langle \bar{u} \rangle_\phi$.

timescale of the turbulence, which for a turbulent pipe flow is proportional to the ratio of pipe diameter to bulk velocity.

E. Swirl Flow

To show the ability of the boundary treatment to affect not only the axial velocity component, swirl was added to the turbulent pipe flow by the body force. The pipe flow in the upstream part of the pipe is identical to the previous case: a nonswirling turbulent pipe flow. The target velocity for the axial component was defined as in the previous case. The azimuthal velocity component of the target velocity was defined by an experiment[13] for a swirl number of $S = 0.6$ scaled down by a factor of 2 in order to obtain a weakly swirling flow with the swirl number $S \simeq 0.38$, with S defined as

$$S = \frac{1}{R} \frac{\int_0^R r^2 \langle \bar{u} \rangle_x \langle \bar{u} \rangle_\phi \, \mathrm{d}r}{\int_0^R r \langle \bar{u} \rangle_x^2 \, \mathrm{d}r} \tag{11}$$

where u_x is the axial velocity component, u_ϕ the azimuthal velocity component, and R the radius of the nozzle.

With the maximum velocity difference $\Delta u_\phi = 0.5$ the minimum forcing constant $\sigma_{\min} = 1.84$ can be computed. As in the preceding cases $\sigma = 6.0$ has been used.

Applying this target velocity field to the pipe-flow computation yields the solution for the azimuthal velocity component shown in Fig. 13. The swirl velocity is attained at the end of the forcing region.

The results of the pipe-flow investigation demonstrated that the proposed treatment of the LES outflow conditions with virtual body forces can be used to enforce a mean flow solution at the LES outflow and that the enforced outflow conditions can indeed alter the upstream flowfield.

VI. Validation: Cold Flow of a Swirl Combustor

To validate the proposed method for treating LES outflow conditions for an LES/RANS interface, the method will be applied to a more complex configuration. Whereas the previous test case of pipe flow has shown the feasibility of the priciple of the body force method, the next test case aims to prove that the upstream influence of the proposed outflow treatment is captured.

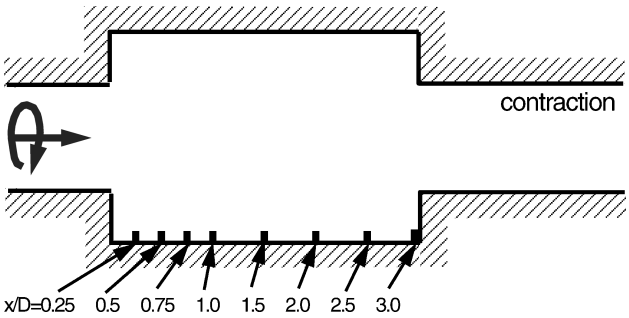

Fig. 14 Swirl flow geometry with contraction.

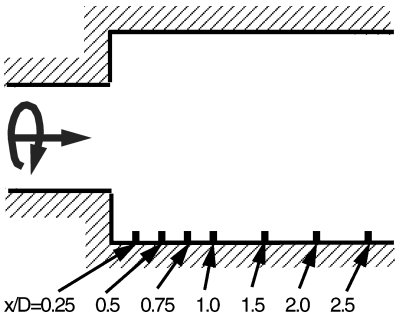

Fig. 15 Reduced swirl flow geometry without virtual body force.

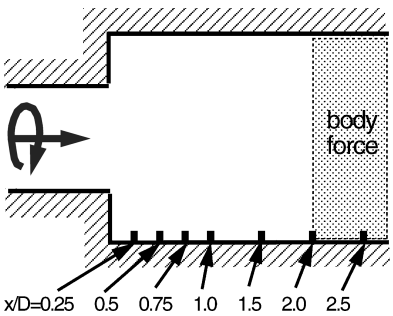

Fig. 16 Reduced swirl flow geometry with virtual body force.

As a test case, the cold flow in an idealized swirl combustor geometry is considered. The geometry consists of an axisymmetric expansion with an expansion ratio of 1:2. The inlet of the computational domain is set $0.5D$ upstream of the expansion, where D denotes the diameter of the pipe upstream of the expansion. The combustion chamber is $3D$ long and ends in a contraction with the same ratio as the expansion 1:2.

The flow at the inlet is swirled with a swirl number $S = 0.38$. As in the swirling pipe flow, the mean azimuthal velocity component is that of an experiment[13] with a swirl number $S = 0.6$ scaled down by a factor of 2. The inflow conditions were created by a auxiliary LES computation of a swirling periodic pipe flow.

The swirl number of $S = 0.38$ has been chosen because it is slightly above the critical limit at which a central recirculation zone develops, and where the flow is believed to be most sensitive to outer influences such as the outflow boundary conditions.[14] Swirl flows are dominated by large-scale turbulence making these flows a field of application of LES par excellence. LES usually achieves high levels of accuracy in predicting swirl flows.[9,15]

To demonstrate the importance of LES outflow conditions and to prove the ability of the proposed LES outflow treatment with virtual body forces to prescribe outflow conditions correctly, three different outflow geometries have been considered: 1) the entire geometry: the swirl flow with the contraction (Fig. 14), 2) a swirl flow where the computational domain is cut off just upstream of the contraction of case 1 at $x/D = 2.75$ (Fig. 15), and 3) the same geometry as in case 2 but with the proposed boundary condition applied in order to simulate the effect of the contraction (Fig. 16).

The mesh size of geometry 1 consists of $384 \times 64 \times 64$ cells, whereas the mesh used for cases 2 and 3 consists of $256 \times 64 \times 64$ cells. The point distribution of both meshes is the same, except for the contraction itself. The smallest cell is near the edge of the expansion and has a edge length of $\simeq 0.005D$. The time-step was determined by the CFL condition and was around $\Delta t \simeq 2.5 \times 10^{-3} \cdot D/u_B$. The computations were running five flowthrough times before flow statistics were recorded. The flow statistics represent the average over two flowthrough times.

Case 1 will be considered as the reference case. Because the computational domain includes the contraction, its influence on the upstream flow will be correctly reflected in the LES solution. For case 2 the computational domain has been reduced and the contraction is outside of the LES domain. Convection boundary conditions are applied at the outflow boundary and the body-forcing method is not applied. Hence, influence of the contraction on the LES flowfield is neglected in case 2. This case is used only to demonstrate

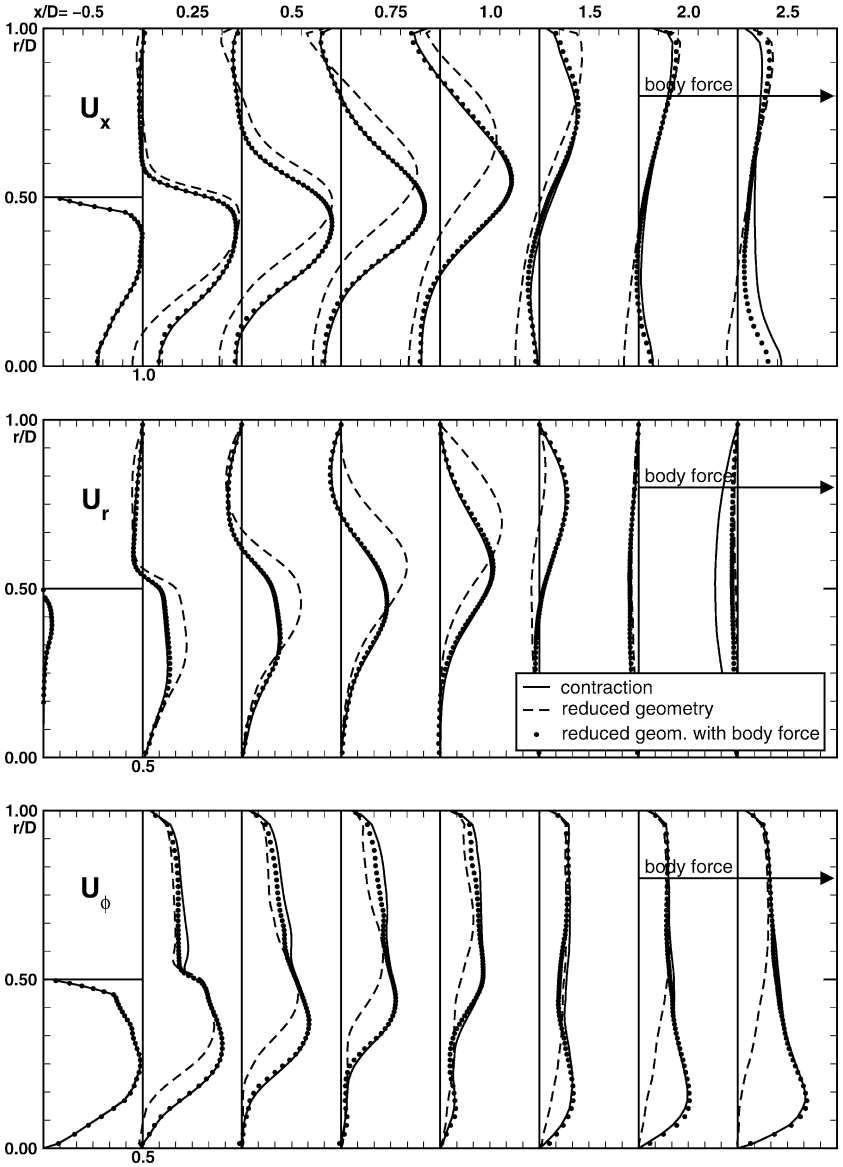

Fig. 17 Velocity profiles for different axial locations: ——, contraction (case 1); – – –, reduced geometry without virtual body force (case 2); and symbols, reduced geometry with virtual body force (case 3).

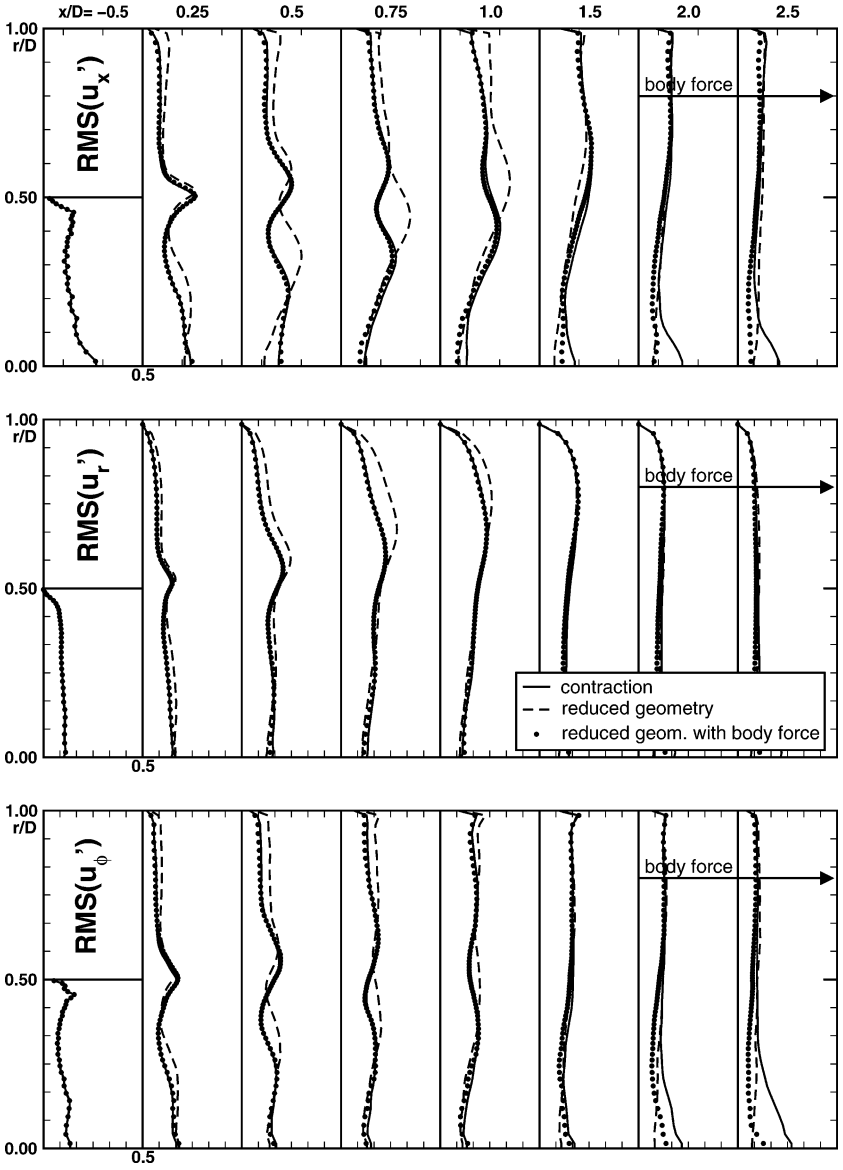

Fig. 18 Profiles of velocity fluctuations for different axial locations: ——, contraction (case 1); – – –, reduced geometry without virtual body force (case 2); and symbols, reduced geometry with virtual body force (case 3).

the influence of the downstream contraction on the flowfield within the entire domain.

Figure 17 shows the mean velocity profiles in cases 1 and 2. It can be seen that the velocity profiles of the computation with the reduced geometry 2 (dashed line) differ from the profiles of the computation of the full geometry 1 (solid line). Hence, it is apparent that the downstream geometry variation has a substantial influence on the entire domain, and that geometry 2 cannot be used to approximate the flow in geometry 1 without special boundary treatment.

To take the contraction outside of the computational domain into account, the proposed outflow boundary treatment is employed in case 3. Instead of using a separate RANS computation, which may introduce another source of error, the Reynolds-averaged velocity profiles from the LES computation of case 1 are imposed on the reduced geometry in the region $x/D = 2.0$–2.5 with virtual body forces. The averaging time span to compute $\langle \bar{u}_i \rangle_{\mathrm{LES}}$ for the body force was $\Delta t_{\mathrm{ave}} = 2D/u_B$, with D the diameter of the pipe upstream of the expansion, and hence, $2D$ the diameter of the combustion chamber and u_B the bulk velocity in the upstream pipe. The forcing constant was set to $\sigma = 8.0$, with $\sigma_{\min} \simeq 2.3$.

Figure 17 shows the mean velocity profiles of case 3 (black dots). It can be seen that not only the velocity profiles inside the virtual-body-force volume adjust, but also the velocity profiles upstream. The LES computation of the reduced geometry with the virtual body force delivers essentially the same prediction as the computation of the entire geometry.

The influence of the LES outflow condition on the turbulent velocity fluctuations is shown in Fig. 18. The different mean velocity distribution caused by the presence of the contraction results in a different turbulence distribution (compare solid line and dashed line in Fig. 18). The employment of the virtual body forces corrects not only the mean velocity field, but also the turbulent quantities (compare solid line and filled circles in Fig. 18). The virtual body force results in an adjustment of the turbulent quantities so that the flow upstream of the body force volume is nearly indistinguishable from the complete computation with the contraction.

The same trend can be observed in the shear stresses (Fig. 19). Because the mean velocity field adjusts to the new outflow conditions, the production and transport of shear stresses adjusts to the new velocity field.

In Fig. 20, the axial pressure distribution on the axis is shown. Caused by the differences in the flowfields of cases 1 and 2, especially in the extend and strength of the recirculation zone, the pressure distribution differs. Although the proposed outflow boundary

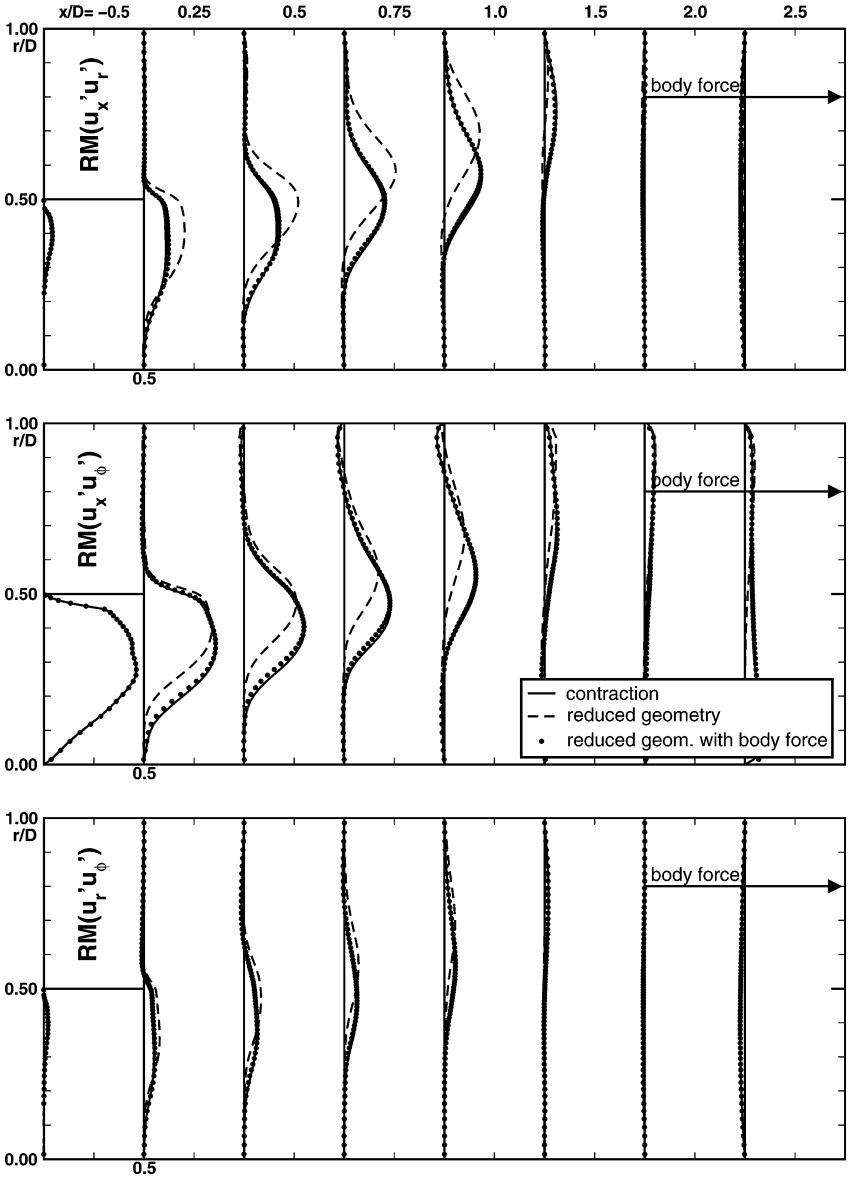

Fig. 19 Profiles of shear stresses for different axial locations: ——, contraction (case 1); – – –, reduced geometry without virtual body force (case 2); and symbols, reduced geometry with virtual body force (case 3).

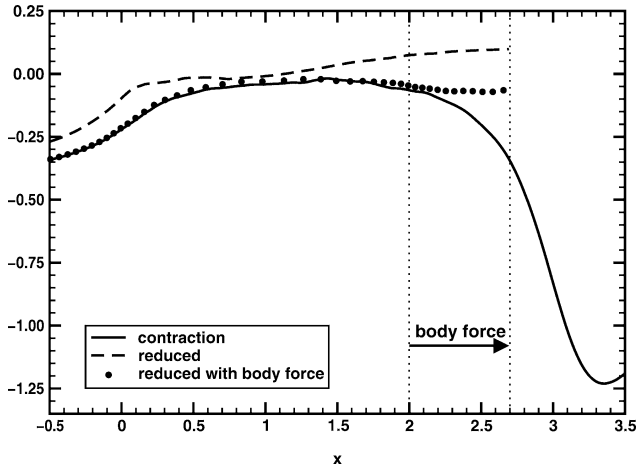

Fig. 20 Axial pressure distribution on the axis: ——, contraction (case 1); – – –, reduced geometry without virtual body force (case 2); and symbols, reduced geometry with virtual body force (case 3).

adjustment by virtual body forces acts only on the velocity components and not on the pressure itself, the pressure distribution adjusts to the correct outflow condition. The pressure distributions from the cases 1 and 3 are in agreement upstream of the body-force volume.

VII. Conclusions

The results of this study show that the outflow conditions may have a major impact on the accuracy of LES computations. Hence, a proper description of the outflow conditions is mandatory.

To avoid the computation of the downstream geometry with LES a method has been proposed to correct the outflow conditions. This method ensures the adjustment of the LES flowfield to the statistical data computed by a downstream RANS flow solver without destroying the resolved turbulent fluctuations.

The adjustment of the LES outflow has an effect throughout the entire flowfield. The resulting prediction of the flowfield is nearly indistinguishable from an LES computation of the entire domain. This allows a drastic decrease in computational costs. Furthermore, it opens up the possibility to use multiple specialized flow solvers

in order to extend the spectrum of physical processes that can be simulated.

Future efforts will use this method in integrated LES/RANS computations for turbomachinery applications.

Acknowledgment

We gratefully acknowledge support by the U.S. Department of Energy under the ASCI program.

References

[1]Veynante, D., and Poinsot, T., "Reynolds Averaged and Large Eddy Simulation Modeling for Turbulent Combustion," *New Tools in Turbulence Modelling*, edited by O. Metais and J. Ferziger, Les Éditions Physique, Springer, Les Houches School, 1996, Chap. 5, pp. 105–140.

[2]Schlüter, J. U., Shankaran, S., Kim, S., Pitsch, H., Alonso, J. J., and Moin, P., "Integration of RANS and LES Flow Solvers for Simultaneous Flow Computations," AIAA Paper 2003-0085, 2003.

[3]Schlüter, J. U., Wu, X., Kim, S., Alonso, J. J., and Pitsch, H., "A Framework for Coupling Reynolds-Averaged with Large Eddy Simulations for Gas Turbine Applications," *Journal of Fluids Engineering* (submitted for publication).

[4]Shankaran, S., Liou, M.-F., Liu, N.-S., and Davis, R., and Alonso, J. J., "A Multi-Code-Coupling Interface for Combustor/Turbomachinery Simulations," AIAA Paper 2001-0974, Jan. 2001.

[5]Pierce, C. D., and Moin, P., "Method for Generating Equilibrium Swirling Inflow Conditions," *AIAA Journal*, Vol. 36, No. 7, 1998, pp. 1325–1327.

[6]Schlüter, J. U., "Consistent Boundary Conditions for Integrated LES/RANS Computations: LES Inflow Conditions," AIAA Paper 2003-3971, June 2003.

[7]Schlüter, J. U., Pitsch, H., and Moin, P., "Large Eddy Simulation Inflow Conditions for Coupling with Reynolds-Averaged Flow Solvers," *AIAA Journal*, Vol. 42, No. 3, 2004, pp. 478–484.

[8]Moin, P., "Progress in Large Eddy Simulation of Turbulent Flows," AIAA Paper 97-0749, Jan. 1997.

[9]Pierce, C., and Moin, P., "Large Eddy Simulation of a Confined Coaxial Jet with Swirl and Heat Release," AIAA Paper 98-2892, June 1998.

[10]Akselvoll, K., and Moin, P., "Large-Eddy Simulation of Turbulent Confined Coannular Jets," *Journal of Fluid Mechanics*, Vol. 315, 1996, pp. 387–411.

[11]Germano, M., Piomelli, U., Moin, P., and Cabot, W., "A Dynamic Subgrid-Scale Eddy Viscosity Model," *Physics of Fluids A*, Vol. 3, No. 7, 1991, pp. 1760–1765.

[12]Moin, P., Squires, K., Cabot, W., and Lee, S., "A Dynamic Subgrid-Scale Model for Compressible Turbulence and Scalar Transport," *Physics of Fluids A*, Vol. 3, No. 11, 1991, pp. 2746–2757.

[13]Dellenback, P. A., Metzger, D. E., and Neitzel, G. P., "Measurements in Turbulent Swirling Flow Through an Abrupt Axisymmetric Expansion," *AIAA Journal*, Vol. 26, No. 6, 1988, pp. 669–681.

[14]Gupta, A. K., Lilley, D. G., and Syred, N., *Swirl Flows*, Energy and Engineering Science, Abacus Press, Tunbridge Wells, England, U.K., 1984, pp. 1–69.

[15]Schlüter, J., Schönfeld, T., Poinsot, T., Krebs, W., and Hoffmann, S., "Characterization of Confined Swirl Flows Using Large Eddy Simulations," American Society of Mechanical Engineers, TURBO EXPO 2001, 2001-GT-0060, June 2001.

K. Ghia
Associate Editor